PCCP

Formation and Migration of H3O+ and OH- Ions at the Water/Silica and Water/Vapor Interfaces Under the Influence of a Static Electric Field: A Molecular Dynamics Study

Journal:	*Physical Chemistry Chemical Physics*
Manuscript ID	CP-ART-07-2020-003656.R1
Article Type:	Paper
Date Submitted by the Author:	21-Sep-2020
Complete List of Authors:	Lentz, Jesse; Rutgers University, Materials Sci. and Eng. Garofalini, Stephen; Rutgers University, Materials Sci. and Eng.

Formation and Migration of H_3O^+ and OH^- Ions at the Water/Silica and Water/Vapor Interfaces Under the Influence of a Static Electric Field: A Molecular Dynamics Study

Jesse Lentz and Stephen H. Garofalini
Interfacial Molecular Science Laboratory
Department of Materials Science and Engineering
Rutgers University

Abstract

The atomistic mechanisms of proton transport under the influence of a static electric field at various angles to the water/silica glass interface were simulated using a reactive, all-atom potential. The fields were shown to change the structure of the 20Å water film significantly, as well as the concentrations and distributions of H_3O^+ and OH^- ions in the film. The field was less than that needed for the dissociation of the water molecule, so the presence of these ions was caused by the interactions with the silica surface. While excess protons at certain silica surface sites can be highly unstable (rattling between adjacent surface sites), protons attached to surface sites that only sample other surface sites are shown to be less mobile in comparison to H_3O^+ and OH^- ions in the water film. After creation of H_3O^+ and OH^- at the silica surface, these ions were observed to have greater mobility away from the glass surface compared to near it. Fields parallel to the glass surface were shown to greatly enhance mobilities of OH^- ions. Very high ion mobilities were observed at the water-vapor interface under field orientations of -45° and +45° (relative to the surface plane) respectively. These field orientations are able to pin charges to the vapor interface in addition to dragging them along it. Both vehicular and structural diffusion of the $H_3O^+$and OH^- ions were determined as a function of location in the water relative to the silica and vapor interfaces. The results indicate the importance of the orientation of a field to a glass surface and the water vapor interface on proton and ion transport in unsaturated pores.

Introduction

The conductivity of protons in porous silica had previously received attention due to its possible potential use as an inexpensive proton-conducting solid electrolyte in fuel cells [1]. It was observed that water in wet mesoporous silica caused: (1) increased proton conductivity, (2) protons that originate on SiO_2 surface sites migrate via the adsorbed water phase, and (3) conductivity increases with increasing water content [1, 2]. Daiko, et al. determined that smaller filled pores have significantly higher conductivities than larger unfilled pores, and that saturated 40Å pores have a higher conductivity than saturated 20Å pores, concluding that immobilized water molecules near the SiO_2 interface restrict proton conductivity in the 20Å pores[2]. Conductivity experiments such as these reflect the combined effects of vehicular diffusion and structural diffusion of the H_3O^+ and OH^- ions via the Grotthuss mechanism[3]. Vehicular diffusion indicates motion of the specific H_3O^+ and OH^- ion whereas structural diffusion indicates migration of the charge via proton exchange, forming new ions.

Dorazio, et al. performed diffusivity measurements in a silica pore (240nm) filled with an aqueous KCl solution as a function of filled volume fraction. They found that the self-diffusion coefficient of water, but not those of K^+ or Cl^- ions, is enhanced by the vapor interface. [4]

It is understood that hydronium and hydroxide ions both have enhanced affinities for the water-vapor interface relative to the bulk [5-7], although it has been shown that the H_3O^+ ion prefers the outer surface while the OH^- ion sits inside.[8-10] Such results imply that in an unfilled pore the vapor interface could be a significant proton transport mechanism. DFT MD simulations of the water-vapor interface have shown its structural effects to extend approximately 3Å [11] or 3.5Å [12] from the vapor interface. This interfacial region has been shown, using DFT and classical simulations, to consist of a 2-dimensional hydrogen bond (H-bond) network in which the number of intra-layer H-bonds is enhanced

and the number of inter-layer H-bonds is reduced compared to bulk water. [13, 14] Water molecules at the vapor interface were shown to have longer reorientation times and shorter continuous H-bond lifetimes compared to molecules in the bulk. [12] This is similar to a trend we previously identified in water molecules at the water-silica interface: we observed longer reorientation times, and shorter continuous H-bond lifetimes relative to molecules in the bulk. [15] Giberti and Hassanali have argued that the 2d H-bond network at the vapor interface results in proton transfer chains being confined to the surface [5], and that this vapor interface-confinement is responsible for the enhanced affinity of protons to the surface. Using a non-reactive water potential, Nikzad, et al. found that parallel electric fields decrease the number of H-bonds formed by molecules at the vapor interface, while increasing the surface tension; perpendicular fields increase the number of H-bonds and decrease the surface tension. [16] Using a DFT simulation of a water slab, Creazzo, et al. show that the conductivity of the vapor interface exceeds that of the bulk by about a factor of two in the 0.3 V/Å to 0.4 V/Å regime. In the regime greater than 0.4 V/Å, at which the field is sufficiently strong to fully align bulk molecules, the conductivity of the bulk becomes similar to that of the interface. [17] This suggests that the anisotropic H-bonding structure of the vapor interface is responsible for its enhanced proton conductivity.

Hydronium ions in water are believed to structurally diffuse via a mechanism whose rate-limiting step is the breaking of a hydrogen bond involving a water molecule in the hydronium's second coordination shell. This causes the hydronium to transiently form a Zundel complex with one of its first neighbors, which stabilizes as an Eigen complex upon the formation of a new H-bond [18-20]. Similar behavior was observed in molecular dynamics (MD) simulations of bulk water using the interatomic potential employed in this paper [21]. Ab-initio MD simulations have shown that proton transfer processes tend to occur in bursts involving multiple hops over a short span of time, separated by longer periods of inactivity.[22, 23]

Multiple DFT simulations of bulk water, using both a classical [24] and a quantum mechanical [25, 26] treatment of nuclei, found that hydroxide ions form stable, hyper-coordinated structures in which they accept four H-bonds. Tuckerman, et al. [24, 25] found this hyper-coordinated structure to be planar, whereas Chen, et al. [26] found it to be non-planar. In both cases, OH^- did not structurally diffuse in this hyper-coordinated structure, but did so only after breaking a hydrogen bond, resulting in the OH^- ion accepting 3 H-bonds in a tetrahedral structure (with a weak H-bond donation). Thus, the breaking of a H-bond and transition to a tetrahedral structure was found to be the rate-limiting step to OH^- structural diffusion. It is plausible, therefore, that the local H-bonding environment has an effect on the rate of OH^- structural diffusion.

NMR and QENS studies showed slow translational motion of water in silica pores. [27-30] In one NMR study, proton transfer in wet silica pores larger than 40Å is ten times larger than that in bulk water. [30] Proton transfer from an oxide surface to adjacent water molecules has been observed in a number of studies.[31-37] Electrochemical studies of wet mesoporous silicas showed enhanced proton conduction as a function of pore size. [2, 38-40]

Fayer, et al. discussed slowed water reorientation in the vicinity of an interface[41]. Using the interatomic potential employed in this study, Lentz and Garofalini similarly showed slow water reorientation at the water/amorphous silica interface in MD simulations in comparison to bulk water[15] and provided a physical justification for the difference between the behavior of continuous and intermittent H-bond lifetime autocorrelation functions at the water/amorphous silica interface[15]. The MD simulations also showed an increased acidity of the water molecules adjacent to the interface in comparison to bulk water based on the shortening of the H-bond at the interface and elongation of the covalent bond. Such behavior is consistent with the deep inelastic neutron scattering studies of Pantalei et al. [42] and the increased acidity of molecules at the water/silica interface observed in DFT calculations by Parashar et al. [43] as well as the DFT studies of Sulpizi et al. [44]

Kazoe, et al. [45, 46] found that water confined in 330nm fused silica pores has a dielectric constant which is about one-seventh that of bulk water, implying that water in a pore has less orientational

freedom than bulk water. It was also found that silanol groups have a higher deprotonation rate in the pore compared to the case of a flat silica surface.

It has been shown via second-harmonic generation that water molecules adjacent to a silica surface are highly oriented [47] and computational studies show water molecules with protons pointing towards the surface. [48-50] Proton adsorption sites were successfully modeled using a two-site model, with 81% of sites having a high proton affinity (pKa of 8.5) and 19% of sites having a low proton affinity (pKa of 4.5) [47] , although there is a significant spread in the values of the low pKa's. [51] It was found previously, using the potential employed in the present work, that certain bridging oxygen sites on a hydrated SiO_2 glass surface are able to adsorb protons [52], similar to the results observed in ab-initio calculations. [53-55] Protons on these bridge sites are less stable than protons on SiOH sites, making bridge sites a potentially important reservoir for protons that could contribute to the system's proton conductivity and be a contributor to the low pKa. In addition, these are also sites of apparent negative charge due to the longer Si-O bond lengths.

The current work uses a classical, reactive, all-atom potential that allows for the dissociation of water molecules and silica [42, 56-58], which has been used previously to study hydronium lifetimes in bulk water [21], reactions at the water/silica interface[58] thermal expansion of nanoconfined water [59], the barrier to dissolution of silica in water [60] and hydrogen bonds in bulk water [61] and at the water/silica interface[15]. There have been a large number of simulations of the water/silica interface, as reviewed by Rimola et al. [62], but only a few use reactive water potentials[49, 63-67].

In this work, a series of simulations of a 20Å water film over an amorphous SiO_2 slab were performed in order to clarify the roles with respect to proton conductivity of water near the SiO_2 interface, away from the interface, and at the vapor interface. This system was simulated with electric fields at varying orientations to the SiO_2 surface, and the effect of the field and of its orientation on the structure and dynamics of water were studied in addition to its effects on the mobilities of protons and hydroxide ions. The strength of the field was below that required to dissociate the water molecule in these simulations, so the presence of the H_3O^+ and OH^- ions are caused by the interactions with the glass surface.

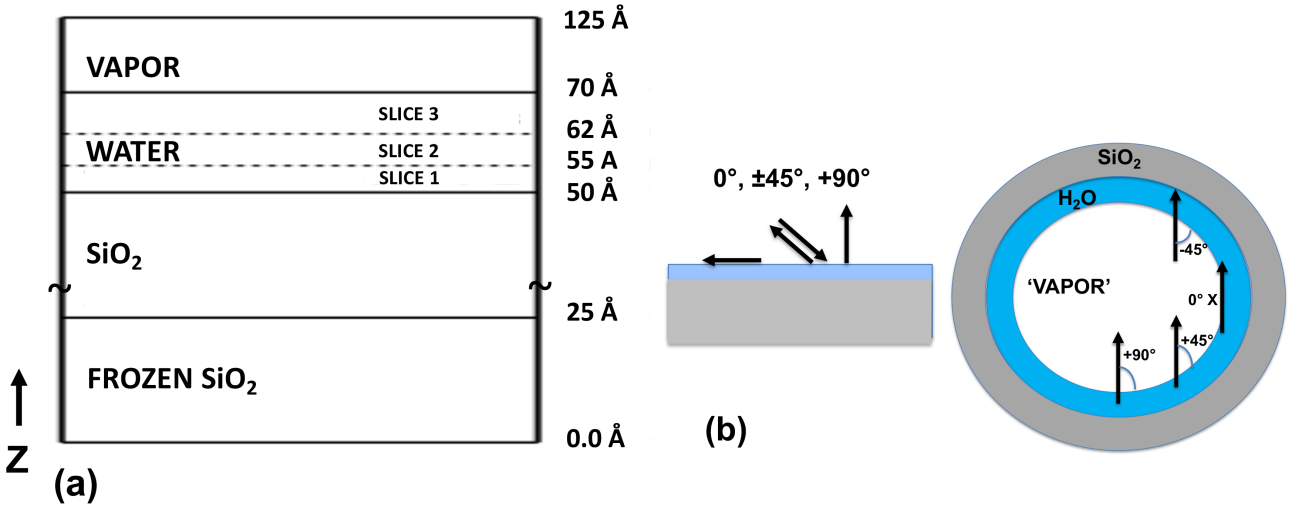

Figure 1: (a) Diagram of the system. The z-distances of the z-slices in the water film are shown. The ~ symbol indicates periodic boundary conditions in the x and y dimensions. The location of the water/vapor interface is approximate, as it undergoes local fluctuations which vary in magnitude between systems. (b) Schematic of the implications of the different angles of the E-fields on the water at a flat surface with water along different locations in a silica pore. (The X at 0° indicates a field parallel to the long axis of a cylindrical pore.)

Computational methods

The current work was done using a classical, reactive, all-atom potential with two-body and three-body terms that has been previous presented [56-58]. A 104Å x 104Å x 50Å silica glass slab, consisting of 12,226 SiO_2 molecules, was prepared through a melt-quench procedure, and a 20Å film consisting of 7,300 water molecules was placed above it. Above the water film is 55Å of vacuum. After being assembled, the system was allowed to react and equilibrate for 4.25 million steps (425ps). Details of the system's preparation have been described previously [15].

The resulting system was then "cleaned" by removing protons from H_3O^+ and bridge sites and placing them on OH^- sites. All the OH^- and H_3O^+ ions in the water were annihilated in the cleaning process, and the system was then equilibrated for an additional 2 million steps (200ps) at a constant temperature of 298K using a canonical-sampling through velocity rescaling (CSVR) thermostat [68] with a time constant of τ=1ps. The equilibrated system was continued for 1ns in the NVT ensemble with electric fields at various angles to the surface. The NVT ensemble was required in the production runs because the field strengths were sufficient to induce electrical currents, which add heat to the systems. A CSVR thermostat was used with τ=500fs. One system had no electric field, while the others had field strengths of 0.05 V/Å at angles (to the surface) of 0°, ±45°, and +90°. This voltage is well below that required for dissociation of the water molecule, which is above 0.25 V/Å.[69] A positive angle refers to a field which points up from the SiO_2 toward the vacuum interface. Forces on the atoms resulting from the field are shown in equation 1(a-c), where q_i is the charge of particle i, E is the field strength (0.05 V/Å), and θ is the field angle. A diagram of the system is shown in figure 1a, and the implications of the e-field angles on the water in a partially filled silica pore are shown in 1b.

$$F_{ix} = q_i E \cos\theta \qquad 1a$$
$$F_{iy} = 0 \qquad 1b$$
$$F_{iz} = q_i E \sin\theta \qquad 1c$$

The water film was divided into three z-slices, with boundaries chosen so that each z-slice contains approximately one third of the initial system's neutral water molecules. A vacuum interface exists above the water, which we often call the 'vapor' interface, although few molecular species move away for this interface as a 'vapor'. In addition to these 3 slices, water molecules (as well as H_3O^+ and OH^- ions) that were directly hydrogen bonded to surface sites, either as donors or acceptors, were labeled W_1 molecules. Hydrogen bonding to the surface was determined using the topological definition of the hydrogen bond[70] and presented in our previous simulations[61]. Distributions of water molecule orientations, hydrogen bond lifetimes, and mean-squared-displacement (MSD) curves were obtained for interfacial water (W_1) and for non-interfacial water as a function of z-slice.

Displacements of positively and negatively charged species were tracked using MSD curves. In this work, positive species include H_3O^+ ions, Si-OH_2^+ sites, and Si-OH^+-Si sites. Negative species include OH^- ions and Si-O^- sites. All charged species present at a set of initial times (t_0) were tracked for the following 50ps or until neutralization with an oppositely charged species. 950 evenly-spaced "t_0" trajectories were averaged: 1 every picosecond for the first 950ps of the run. Squared displacements of charge locations (specifically, the location of the central oxygen atom associated with an ion or charged surface group) were used to obtain MSD curves.

The MSD curves were calculated by the following procedure. Let O_a be an oxygen hosting an excess charge at time t_0. If the excess charge remains on O_a at a later time t_1, the charge's displacement is O_a's position at t_1 relative to its position at t_0. If O_a has transferred its excess charge (via proton transfer) to another oxygen O_b between times t_0 and t_1, the charge's displacement is O_b's position at t_1 relative to O_a's position at t_0. If O_b then transfers its charge to another oxygen O_c between times t_1 and

t_2, the charge's displacement is O_c's position at t_2 relative to O_a's position at t_0; the entire chain of transfers is regarded as a single propagating charge.

Translational motion of ions and proton transfers both contribute to the calculated charge displacements, and thus these MSD curves measure the combined effects of surface hopping, structural diffusion, and vehicular diffusion. Surface hopping entails a proton transfer from a positively charged surface site (Si-OH^+-Si or Si-OH_2^+) to a neutral surface site (Si-O-Si or Si-OH), or a transfer from a positively charged surface site to an adjacent interfacial H_2O molecule. A fraction of the SiOH also deprotonate, as presented in previous work using this potential. [58] Structural diffusion entails a transfer within the water from an H_3O^+ to an H_2O or from an H_2O to an OH^-, and vehicular diffusion entails the physical movement of an H_3O^+ ion or OH^- ion within the water. MSD curves were generated for excess charges on the surface (bridge and Si-OH_2^+ sites) as well as for H_3O^+ ions and OH^- ions in the three z-slices of the water film. A charge's trajectory contributes to the MSD curve associated with its site type and z-slice at t_0. If a proton transfer results in the neutralization of a pair of oppositely charged species, the locations of both charges are considered to be fixed at the location of the neutralization reaction for the remainder of the 50ps tracking interval. If the pair re-ionizes within the 50ps tracking interval, their displacements continue to be tracked relative to the locations of the original ions at t_0.

The MSD curves of certain field/z-slice/species combinations were excessively noisy due to low species concentrations; Giberti and Hassanali have commented on the problem of MSDs for proton diffusion processes having large variability [5]. To address this MSD convergence problem, MSD curves are only included for field/z-slice/species combinations for which the 950 t_0 configurations, collectively, contain at least 300 examples to average over. This population cutoff resulted in the discarding of the No-Field and +45° systems' middle-region H_3O^+ MSDs and of the 0° and -45° systems' vapor-interface H_3O^+ MSDs. Due to the large number of H_2O molecules, the MSD data for H_2O are more uniform than those for H_3O^+ or OH^-.

Results and discussion

Water/vapor interface perturbations

The water/vapor interface can show short-lived surface roughness in the No-field, 0°, and +45° systems, but the +90° and -45° fields produce different behavior. The density profiles in figure 2 show that there is a small density increase at the glass/water interface (~4%) in almost all cases, similar to previous studies of the glass/water interface with no E-field. [59, 71] A lower density increase is observed at the water/vapor interface (< 1%), which is quite different from the value observed by Creazzo et al. in their ab-initio calculation of the water/vapor interface. [17] There, they observed a density increase of ~40% under their E-field (~5x stronger than the one we use here) parallel to the interface. This may be due to their small system size of 256 molecules and 19.7Å in length and short time (30ps per E-field). There is a moderate elongation of the density profile in the +Z direction for the +90° and -45° fields, while the other field orientations maintain a relatively flat vapor interface. This can be seen graphically in figure 3 for the +90° system.

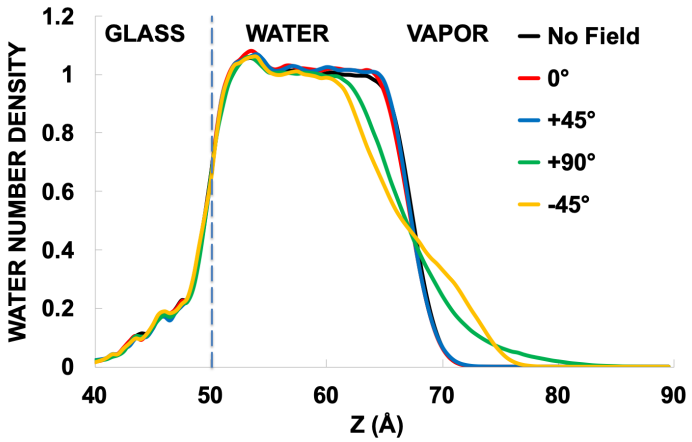

Figure 2. Density profiles of water as a function of the different E-field orientations.

Figure 3 shows the top and side views of the +90° system at the start and end of the run. Water z-slices 1 and 2 are shown in pink; z-slice 3 is shown in blue for water below 70Å and green for water above 70Å; a section of the silica surface in shown in grey. Note that water (pink) has diffused about 10Å into the silica (grey) along specific 'channels'. Waters in z-slice 3 below 70Å decrease in density as shown by the density profile (figure 2) and the increase in pink visible in the top view image in figure 3 at the end of the run. Due to the +90° field, there is a surface perturbation that causes some waters to move in the +Z direction (green); other 'blue' waters follow these waters and form a cluster that moves upward under the field. This creates a low density of waters in the original z-slice 3. Such a low density can play two dissimilar roles in the dynamics of the water and ions. It is known that water at a higher density enhances proton transfers. [72, 73], so this lower density may be expected to decrease proton transfers in z-slice 3, which affects structural diffusion of the ions. However, the lower density may concurrently increase vehicular diffusion of the ions. In fact, for the OH^- ions vehicular diffusion dominates in all systems and all field orientations, with the difference between structural and vehicular diffusion being greater farther from the silica surface.

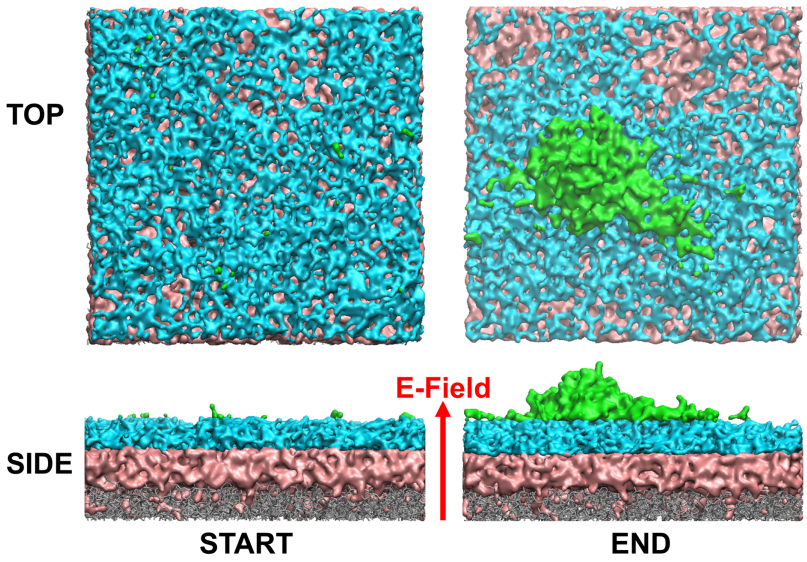

Figure 3. Top and side views of the +90° field at the start and end of the 1ns run. Z-slices 1 and 2 in pink; z-slice 3 in blue and green over portion of glass surface (grey). The field causes water migration and cluster formation outward into the 'vapor'.

Vehicular diffusion has been shown to dominate for the OH^- ion. [74] However, the H_3O^+ ions show varied behavior with respect to the diffusion mechanism for the different layers and field orientations.

Despite the surface roughness observed under the +90° and -45° fields, the distribution of water molecules among the three z-slices remains nearly unchanged and hence the interpretation of the three z-slices remains intact. However, such surface instability under a perpendicular field would have important implications in unsaturated pores and its potential to enhance ion migration in such pores will be the subject of future work.

Surface sites and ion concentrations

Positively charged surface sites include Si-OH-Si (proton on bridging O between 2 Si) and $Si\text{-}OH_2$ at moderately low concentrations. Si-OH-Si sites in all systems had time-averaged concentrations within the range 0.56 ± 0.14 / nm^2, which is about one-tenth of the concentration of SiOH sites (as expected with this potential, the SiOH sites are ~5/ nm^2). Si-OH-Si concentrations for each system are shown in figure 4: relative to the system with no field, the -45° field increases the concentration of Si-OH-Si sites by about 40%, whereas the upward and parallel fields decrease the concentration by about 14%. This agrees with the intuitive expectation that an upward field (parallel to the

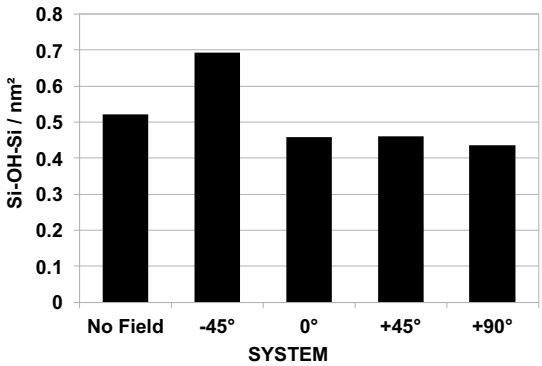

Figure 4. Time-averaged concentrations of protonated bridge sites (Si-OH-Si) in each of the five systems.

surface normal) would shift the equilibrium concentration of Si-OH-Si sites to favor de-protonation, while a downward field would favor protonation from the adjacent water molecules. The concentrations of Si-OH_2 sites, 0.05 ± 0.01 / nm^2, are about one-tenth the concentration of Si-OH-Si sites. No statistically significant relation between field orientation and Si-OH_2 concentration was observed. However, there is a correlation between the increase in the concentration of protonated bridge sites (Si-OH-Si) in the -45° field and the number of OH^- ions that form, as discussed below with respect to figure 5a.

Proton transfers and ion formation occurring in the water/silica interfacial system was previously discussed in detail. [15, 58] SiOH sites are considerably more stable with respect to proton transfers but do show deprotonations on the order of 14% for different configurations of the water/silica systems (flat surfaces) [58] although many of these deprotonations are short-lived events indicative of rattling.

Adsorption of protons by bridge sites led to a positive surface charge on the glass in all systems. Proton adsorption by bridge sites has been the subject of previous work using this potential [52]. Such protons are only stable on bridging O at sites with Si-O-Si angles near 135° (which is less than the average siloxane bond angle of 150°), with a binding energy of ~ 30 kcal/mole. Both of these simulation results are consistent with ab-initio calculations[53, 54]. Others have similarly observed protons on such bridging oxygen in silica. [55, 75, 76] Bridge protonation produces an increased concentration of OH^- ions in the water. The average number of OH^- ions for each system is shown in figure 5a. Field orientation had a significant effect on both the concentrations and locations of OH^- ions. As expected, concentrations of OH^- ions in the water correspond to concentrations of protons adsorbed on the glass due to the dissociation of a water molecule adjacent to the glass surface. The dissociation of water at such bridging oxygens indicates an enhanced acidity of the water molecules adjacent to such sites, consistent with the increased acidity of acid molecules adjacent to the silica surface. [43] It should be noted that Vacha et al. [77] found both H_3O^+ and OH^- affinity near a hydrophobic hydrogenated C wall, with more OH^- forming than H_3O^+. We would expect a greater affinity near a hydrophilic wall, where H-bonding would assist this affinity and certain O sites would attract a proton. In comparison to the 'No Field' system, the -45° field increases the concentration of OH^- ions in the water film by 49%, while the upward field decreases the concentration by 28%. As shown in figure 5a, -45° field significantly increases the concentration of OH^- ions near the vapor interface (z-slice 3), while upward fields significantly decrease it. By comparison, concentrations of OH^- ions near the glass interface are less sensitive to field orientation.

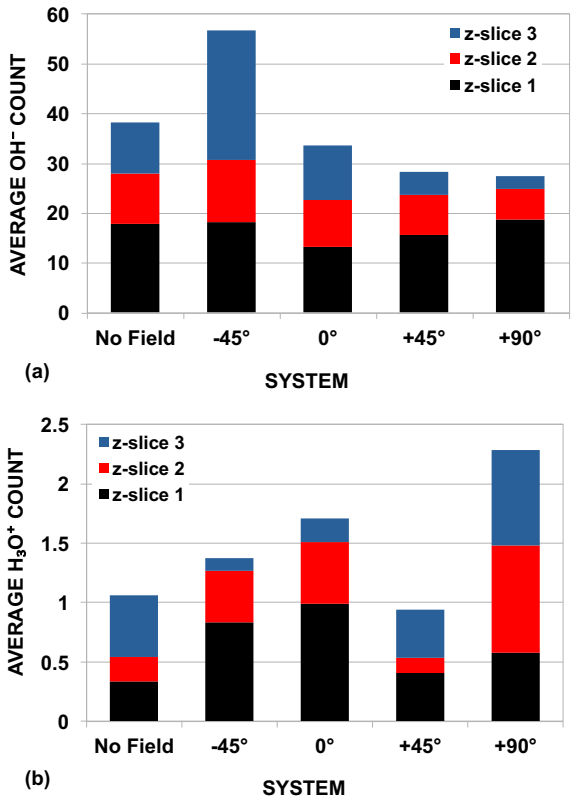

Figure 5. Counts of time-averaged (a) OH^- and (b) H_3O^+ ions in each of the five systems, by z-slice.

The concentration of OH^- ions in the water implies an inordinate increase in pH, as would occur for all simulations that show even one OH^- ion (or one H_3O^+ ion that would decrease solution pH) given the small system sizes.

Counts of H_3O^+ ions, shown in figure 5b, were comparatively low due to the high concentrations of OH^- ions available to neutralize them. In the No Field system, H_3O^+ ions have an enhanced affinity for the water-vapor interface relative to the lower and middle regions, in agreement with the results of DFT simulations [5, 7]. -45° and 0° fields reverse this affinity; in these systems, the water-vapor interface has a greatly decreased concentration of H_3O^+ ions relative to the lower and middle regions. This is expected in the case of -45° field (its enhanced concentrations of OH^- ions at the vapor interface causes increased neutralization of H_3O^+ ions), but the interpretation in the case of the parallel field is less obvious. Also, while the +90° system has an enhanced concentration of H_3O^+ as expected, the +45° system has an anomalously low concentration of H_3O^+. Although one may expect an upward field to cause an enhanced concentration of H_3O^+ at the vapor interface relative to the lower and middle regions (z-slice 1 and z-slice 2, respectively), the +90° system does not exhibit this behavior.

Giberti and Hassanali argue that hydronium's affinity for the vapor interface is due to the anisotropy of the H-bond network at the interface. [5] Thus, plausible explanations for the aforementioned trends are that the parallel field induces anisotropy in the middle region, and that the upward field disrupts the parallel structure of the vapor interface, causing protons in both cases to have reduced affinity for the interface compared to the No Field system. These structural effects will be demonstrated in the following section.

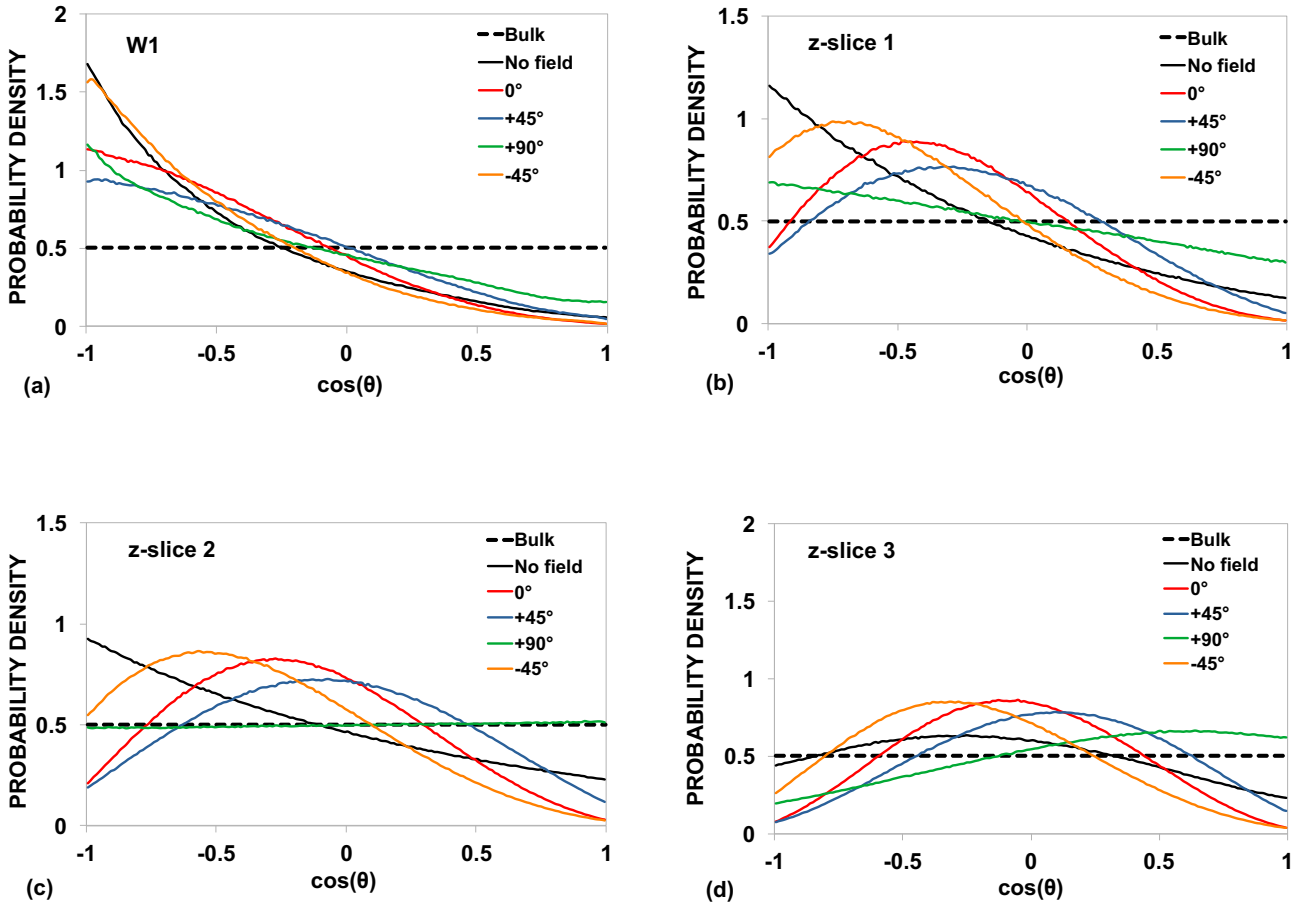

Figure 6. Distributions of molecular dipole moment angles by system for (a) W1 water molecules, and for non-W1 water molecules in the (b) first, (c) second, and (d) third z-slices.

Structure

Distributions of dipole orientations relative to the +Z axis of neutral water molecules are shown as probability density functions in figures 6a–6d. Water molecules H-bonded to the glass surface (W1) are pointed downward in all fields, although the +90° systems enhances upward orientations (downward indicates the dipole direction points at an angle greater than 90° from the +Z direction). In the No-Field system, a downward orientation is favored to some extent in all slices, with this preference being strongest at the glass interface and weakest at the vapor interface. In agreement with prior work [12-14, 78], an almost parallel but slightly downward orientation is preferred near the vapor interface (z-slice 3) in the No-Field system. This can be inferred from the peak at cos(θ)=-0.25 (θ=104.5° to the surface normal). Brown, et al. find a slightly upward-facing modal orientation of 78° to the surface normal. [6]

As expected, when moving from the glass interface to the vapor interface, the peak maximum in the probability density for each z-slice shifts toward the positive angular direction for the -45°, 0° and +45° systems, as shown in figure 6b, 6c, 6d. At the vapor interface (z-slice 3), parallel and oblique fields (0° and ±45°) enhance the preference for a parallel structure, and these fields extend this parallel-preferred structure into the middle region (z-slice 2). Even in z-slice 1, the parallel and oblique systems all have modal orientations that are oblique rather than purely downward. As noted earlier, this induced anisotropy in the middle region offers a possible explanation for hydronium's lack of affinity for the vapor interface in these systems. The +90° field diminishes the downward preference at the glass interface and induces a small upward preference at the vapor interface. Surprisingly, it produces a nearly isotropic, bulk-like distribution of orientations in the middle region. This can be understood as a "confused region" between two interfaces that have opposing modal orientations.

To summarize, both the 0° and ±45° fields enhance the structural effect of the vapor interface on the water and extend the effect to the glass interface. The +90° field diminishes the structural effect of the glass interface on the water and produces a bulk-like structure in the middle region. Previous work [5, 17] suggests that induced structural anisotropy should be associated with enhanced proton conductivity due to the formation of H-bond wires along the direction of the induced anisotropy.

Hydrogen bond dynamics

The effect of the fields on the water's dynamics is reflected in the intermittent H-bond lifetime autocorrelation functions (c(t)), shown in figure 7a through 7c for interfacial water (W1). Compared to the No Field system, the +90° field causes slightly shorter H-bond lifetimes at the glass interface. The 0° field causes significantly longer lifetimes at the glass interface. Lifetimes in the +45° field system is consistent with the combined effects of the 0° field and the +90° field.

Note that the c(t) values in the vertical axes are different in figures 7a-c, showing significantly longer lifetimes from surface to W1 waters in 7a, followed by W1 to surface sites in 7b, with the shortest lifetimes between W1 waters and other waters in 7c. Such behavior is consistent with and an

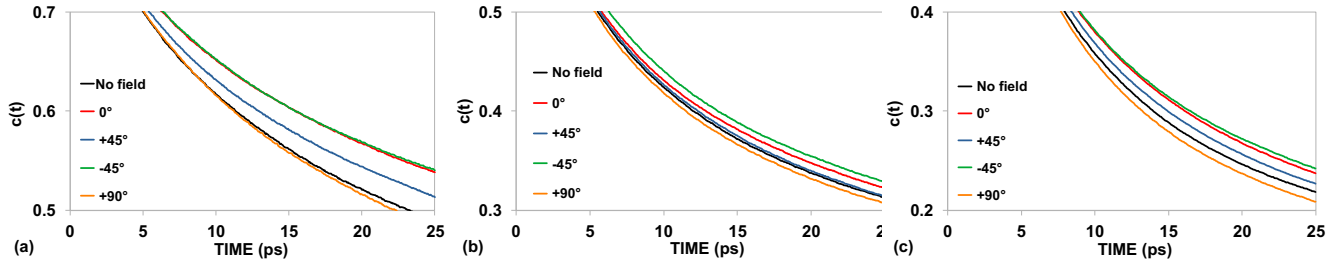

Figure 7. Intermittent H-bond lifetime autocorrelation functions of interfacial water, for (a) glass-to-W1 H-bonds, (b) W1-to-glass H-bonds, and (c) W1-to-water H-bonds.

expansion of our previous results describing the intermittent H-bond lifetime autocorrelation functions for water adjacent to the amorphous silica surface[15].

Intermittent H-bond lifetime autocorrelation functions for non-interfacial water (z-slices 1 to 3) are shown in figures 8a through 8c. The +90° field has no noticeable effect in the lower and middle regions and causes shorter H-bond lifetimes at the vapor interface. The 0° field causes longer lifetimes at the glass interface (consistent with its effect on interfacial H-bond lifetimes), slightly longer lifetimes in the middle region, and significantly longer lifetimes at the vapor interface. The -45° field, similar to the interfacial case, is consistent with the combined effect of the 0° field and the +90° field.

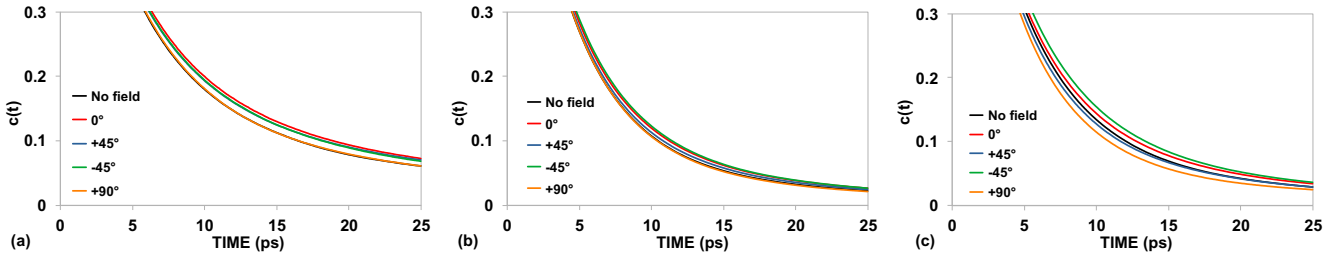

Figure 8. Intermittent hydrogen bond lifetime autocorrelation functions of non-interfacial water, for donor molecules within the (a) first, (b) second, and (c) third z-slices.

As noted in the introduction, Pezzotti, et al. have reported shorter continuous H-bond lifetimes and longer reorientation times (relative to the bulk) at the vapor interface [12], a trend similar to what we have previously observed in water molecules at the silica interface. [15] This may suggest that structural anisotropy generally causes librational amplitudes (ability to transiently break H-bonds) to increase, while causing non-librational reorientation (as measured in the present work by intermittent H-bond lifetimes at the picosecond timescale) to slow down. This would explain why the +90° field decreases intermittent H-bond lifetimes at the vapor interface (it decreases the interface's anisotropy).

Mechanisms of charge transport

We consider several mechanisms of charge transport: interfacial proton hopping, and diffusion of H_3O^+ and OH^- in the water (including both structural and vehicular diffusion) near the glass, in the middle region, and near the vapor interface. Previous results showed significant rates of proton transfers involving surface sites, greatly exceeding the rate of proton transfers in bulk water. [15] Detailed analysis of the proton transfer chains reveals that the majority of surface transfers are just "rattling", and that only a small fraction of the rattling protons on the surface participate in long-range charge

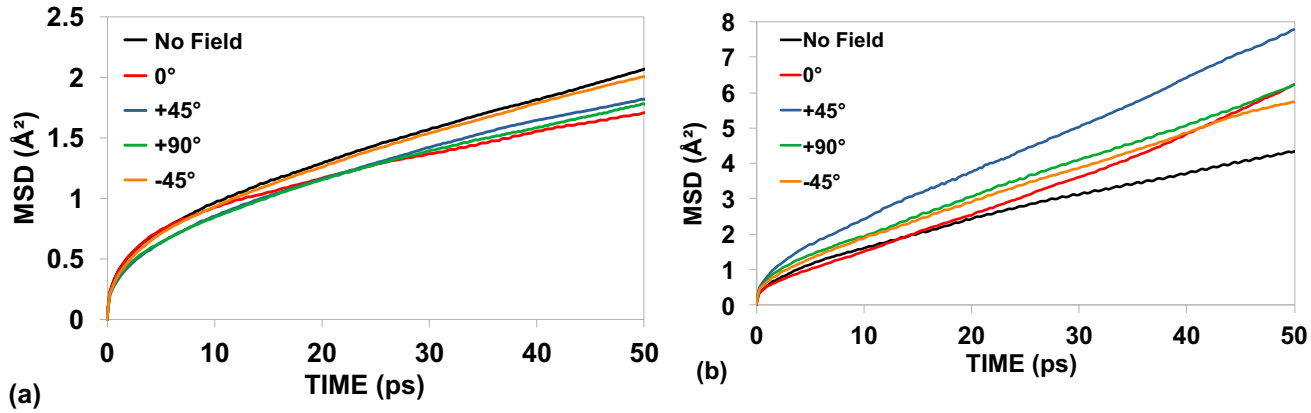

Figure 9. MSD curves of positive charges on (a) Si-OH-Si and (b) Si-OH_2 sites on the glass surface. Note difference in Y-axis value.

displacement during the timescale of the simulation. This immobility of surface charges is quantified in the current work using MSD curves.

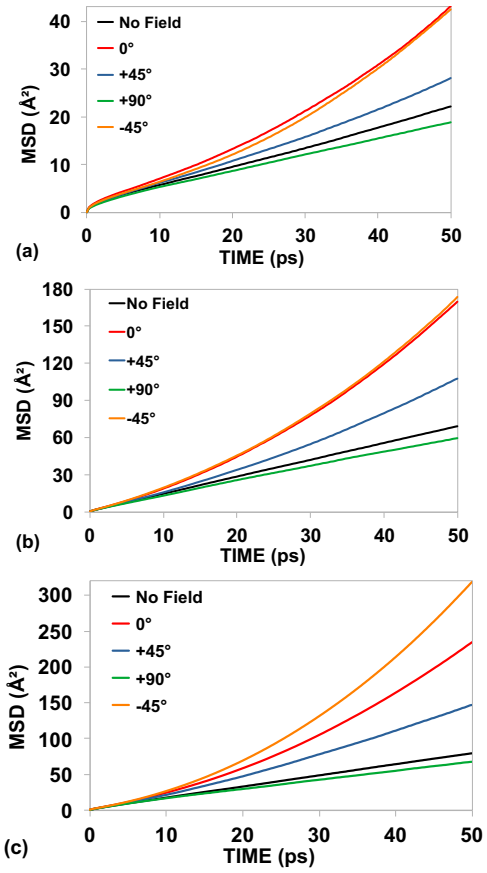

Figure 10. MSD curves of OH^- ions in the (a) first, (b) second, and (c) third z-slices. Note difference in Y-axis value.

MSD curves of charges at different sites and locations are shown in figures 9-11. Figures 9a and 9b correspond to Si-OH^+-Si and $SiOH_2^+$ charges respectively. $SiOH_2^+$ charges have greater mobility than Si-OH^+-Si charges because they are less stable and hence more likely to transfer. About 15% of Si-OH^+-Si protons neutralize within 50ps, 84% remain on the same bridge site or transfer to another bridge site, and about 1% of them transfer to interfacial water and become H_3O^+ ions. This increase in H_3O^+ ions caused by the interface is consistent with our earlier studies [58] and provides a plausible explanation of the enhanced proton conduction in wet mesoporous silica observed experimentally. [2] In the case of $Si\text{-}OH_2^+$, within 50ps, about 14% lose a proton which neutralizes with a negative charge, 14% move to a bridging oxygen to form an Si-OH^+-Si site, and about 3% transfer to interfacial water and become H_3O^+; 68% either remain on the same $SiOH_2^+$ site or transfer to another SiOH to form a new $SiOH_2^+$. All field orientations appear to increase the charge mobility of $SiOH_2^+$ sites. No conclusive relation between field orientation and the charge mobility of Si-OH^+-Si sites was observed.

MSD curves of OH^- ions near the glass surface, in the middle region, and near the vapor interface (z-slices 1, 2, 3 respectively) are shown in figures 10a–10c respectively. Mobilities of OH^- in all three regions significantly exceed mobilities of positive surface charges. At the silica interface, however, the OH^- have very low mobilities. In all systems, OH^- mobilities in the middle region are enhanced by a factor of ≥ 2 compared to near the glass surface, and mobilities near the vapor interface are enhanced even further. Parallel and -45° fields cause particularly high mobilities, enabling OH^- ions to glide in the low-density region near the vapor interface. The -45° field (which pulls negative charge toward the vapor interface) produced the greatest mobility in this region because it has the dual effect of pinning OH^- ions to the vapor interface as well as dragging them along this interface. We also note that the concentration of OH^- ions near the vapor interface is enhanced in the case of the -45° fields (figure 5a); taken together with the overall high concentration of OH^- in the system, this implies that OH^- gliding near the vapor interface is by far the most significant contribution to system conductivity in the case of

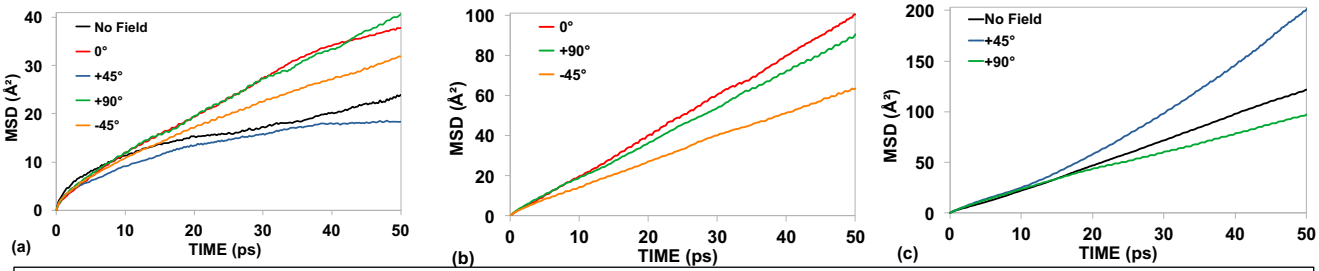

Figure 11. MSD curves of H_3O^+ ions in the (a) first, (b) second, and (c) third z-slices; the MSD curve of H_3O^+ in bulk water is shown for reference. Note difference in Y-axis values.

a 0° or -45° field. In all regions, the lowest OH^- mobilities were observed under the +90° field (which pulls OH^- toward the glass), followed closely by mobilities under no field.

H_3O^+ MSD curves are shown in figures 11a–11c, again for H_3O^+ near the glass, in the middle region, and near the vapor interface respectively. Two systems were omitted from 11b and two from 11c because the corresponding H_3O^+ populations were too low to produce reliable MSD curves. H_3O^+ mobilities in all regions are significantly higher than those of surface-bound protons. As in the case of OH^-, mobilities increase farther from the glass, implying that proton transport in the first z-slice (within about 5Å of the glass) is limited compared to water farther from the glass. This is consistent with the results of Daiko, et al. [2], which imply that the conductivity of saturated 40Å SiO_2 pores is about two orders of magnitude greater than that of saturated 20Å pores. In a 40Å pore, about 44% of the pore's water is within the slowed-down region within 5Å of the glass, whereas in the 20Å pores, 75% of the pore's water is within this region.

In the absence of a field, the mobilities of H_3O^+ and OH^- are similar and low near the glass surface, whereas the mobility of H_3O^+ is higher by a factor of 1.5 near the vapor interface. Under a 0° field, mobilities of OH^- exceed those of H_3O^+ by factors of 3.4 and 2.5 near the glass surface and in the middle region, respectively. Maximal mobility of H_3O^+ ions occurs under the +45° field near the vapor interface. Similar to OH^- under a -45° field, this +45° field pins H_3O^+ ions to the vapor interface in addition to dragging them along it. However, mobilities at the vapor interface of OH^- under the -45° field exceed those of H_3O^+ under the +45° field by a factor of 1.9. The +90° field lowers the mobility of H_3O^+ near the vapor interface, which is consistent with the its effect at the vapor interface on the structure of water. The field imparts an upward (+Z direction of the dipole) orientation of the molecules that disrupts the 2d interfacial H-bond network, and previous work suggests that this 2d H-bond network enhances structural diffusion of H_3O^+ at the vapor interface. [5, 17]

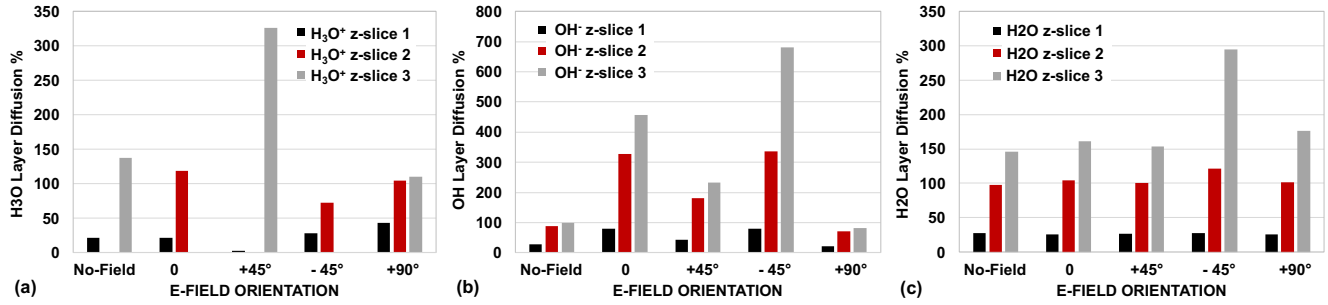

Figure 12. Relative diffusion coefficients of species as a function of E-field orientation for: (a) H_3O^+ diffusion per z-slice, (b) OH^- diffusion per z-slice, (c) H_2O diffusion. Data are relative to bulk water values for each specific species. Note Y-axis values.

Figure 12(a-c) shows diffusion coefficients, calculated from the MSD curves, relative to the bulk water diffusion coefficients calculated using this potential for each particular species. Near the glass surface (z-slice 1), H_3O^+ (12a) and OH^- (12b) ions and H_2O molecules (12c) all have lower mobilities of their respective species than that in bulk water. The H_2O molecules near the glass surface are severely constrained with the same relative values (~25%) for all systems. Low water diffusivity near the glass surface has been shown in the past. Away from the glass surface, mobilities of H_3O^+ and OH^- are comparable to, exceed, or greatly exceed their respective bulk water values, according to the previously discussed field-orientation-specific effects. In z-slice 2, the H_2O molecules have values very similar to bulk water. At the water/vapor interface, the diffusivities of water molecules are about 1.5 times that of bulk water in all systems except the -45° system, in which it is about 3 times that of bulk water.

This large relative diffusion coefficient in the -45° field also occurs for the OH^- ions. A question arises as to whether the OH^- ions pull the H_2O molecules in the -45° field or vice-versa. However, the

H_2O molecules have very similar diffusion coefficients in all systems and layers (except z-slice 3 at -45°), whereas the OH^- ions have very different diffusion coefficients for the different systems and layers. In addition, the concentrations of OH^- ions in the systems are low in comparison to the number of H_2O molecules. Thus, the diffusion of the OH^- and H_2O seem to be independent of each other.

Conclusion

Electric fields at varying orientations to the glass surface were shown to impart distinct structural effects on a 20Å water film over a glassy SiO_2 surface: a parallel field enhances the anisotropy of the water/vapor interface, and an upward field imparts an upward orientation to water molecules at the vapor interface while creating a structurally isotropic region in the middle of the film. While it has previously been shown that protons at certain surface sites can be highly unstable with respect to proton transfer (rattling between adjacent surface sites), protons bound to surface sites show significantly less long-range mobility on the surface in comparison to H_3O^+ and OH^- ions in the water away from the silica surface. Since the static E-field is below that needed for the dissociation of a water molecule, these H_3O^+ and OH^- ions are caused by interactions between the water and the silica surface. Ions near the glass interface are shown to have lower mobilities relative to the middle and upper regions of the water film. Structural and vehicular diffusion of the ions contribute differently in different regions of the water. Despite increasing the concentration of H_3O^+ at the vapor interface, the upward field decreases their mobility there because the structure becomes less conducive to proton transfer. The parallel (0°) field is shown to rapidly transport OH^- ions in the middle and upper regions of the water film. At the vapor interface, -45° and +45° fields cause rapid transport of OH^- and H_3O^+, respectively, because these fields have the dual effect of pinning charges near the vapor interface and of dragging them along it. Given this enhancement of H_3O^+ and OH^- structural and vehicular diffusion by the vapor interface at appropriate electric field angles, a substrate with a random network of large-diameter, partially filled pores may offer superior performance as a proton conducting electrolyte compared to saturated pores. While our results indicate that proton transport is slowed down within about 5Å of a glass surface, consistent with a slowing of diffusion of water molecules at the glass surface, there is a large increase in the concentration of H_3O^+ and OH^- ions at the water/glass interface that affect overall proton conductivity under electric fields. The effect of structural perturbations of the water/vapor interface caused by specific E-field orientations could have important implications on behavior in pores and will be addressed in further studies.

Conflicts of interest

There are no conflicts of interest.

Acknowledgements

The authors acknowledge support from the National Science Foundation Environmental Chemical Science Program of the Division of Chemistry, grant number 1609044.

References

1. H. B. Li and M. Nogami, *Adv. Mater.*, 2002, **14**, 912-914.
2. Y. Daiko, T. Kasuga and M. Nogami, *Microporous Mesoporous Mater.*, 2004, **69**, 149-155.
3. B. Halle and G. Karlstrom, *J. Chem. Soc., Faraday Trans. 2*, 1983, **79**, 1047-1073.
4. F. Dorazio, S. Bhattacharja, W. P. Halperin and R. Gerhardt, *Phys. Rev. B*, 1990, **42**, 6503-6508.
5. F. Giberti and A. Hassanali, *J. Chem. Phys.*, 2017, **146**, 244703.
6. E. C. Brown, M. Mucha, P. Jungwirth and D. J. Tobias, *J. Phys. Chem. B*, 2005, **109**, 7934-7940.
7. H. S. Lee and M. E. Tuckerman, *J. Phys. Chem. A*, 2009, **113**, 2144-2151.

8. B. Winter, M. Faubel, I. V. Hertel, C. Pettenkofer, S. E. Bradford, B. Jagoda-Cwiklik, L. Cwiklik and P. Jungwirth, *J. Am. Chem. Soc.*, 2006, **128**, 3864-3865.
9. P. Jungwirth and B. Winter, *Annu. Rev. Phys. Chem.*, 2008, **59**, 343-366.
10. M. Mucha, T. Frigato, L. M. Levering, H. C. Allen, D. J. Tobias, L. X. Dang and P. Jungwirth, *J. Phys. Chem. B*, 2005, **109**, 7617-7623.
11. M. Sulpizi, M. Salanne, M. Sprik and M. P. Gaigeot, *J. Phys. Chem. Lett.*, 2013, **4**, 83-87.
12. S. Pezzotti, A. Serva and M. Gaigeot, *J. Chem. Phys.*, 2018, **148**, 174701.
13. S. Pezzotti, D. R. Galimberti and M. Gaigeot, *J. Phys. Chem. Lett.*, 2017, 3133-3141.
14. A. Serva, S. Pezzotti, S. Bougueroua, D. R. Galimberta and M. Gaigeot, *J. Mol. Struct.*, 2018, **1165**, 71-78.
15. J. Lentz and S. H. Garofalini, *Phys. Chem. Chem. Phys.*, 2019, **21**, 12265-12278.
16. M. Nikzad, A. R. Azimian, M. Rezaei and S. Nikzad, *J. Chem. Phys.*, 2017, **147**, 204701.
17. F. Creazzo, S. Pezzotti, S. Bougueroua, A. Serva, J. Sponer, F. Saija, G. Cassone and M. Gaigeot, *Phys. Chem. Chem. Phys.*, 2020, 10438-10446.
18. N. Agmon, *Chem. Phys. Lett.*, 1995, **244**, 456-462.
19. D. Marx, M. E. Tuckerman, J. Hutter and M. Parrinello, *Nature*, 1999, **397**, 601-604.
20. T. J. F. Day, U. W. Schmitt and G. A. Voth, *J. Am. Chem. Soc.*, 2000, **122**, 12027-12028.
21. G. K. Lockwood and S. H. Garofalini, *J. Phys. Chem. B*, 2013, **117**, 4089-4097.
22. A. Hassanali, M. K. Prakash, H. Eshet and M. Parrinello, *Proc. Natl. Acad. Sci. U.S.A.*, 2011, **108**, 20410-20415.
23. A. Hassanali, F. Giberti, J. Cuny, T. D. Kuhne and M. Parrinello, *Proc. Natl. Acad. Sci. U.S.A.*, 2013, **110**, 13723-13728.
24. M. Tuckerman, K. Laasonen, M. Sprik and M. Parrinello, *J. Chem. Phys.*, 1995, **103**, 150-161.
25. M. E. Tuckerman, D. Marx and M. Parrinello, *Nature*, 2002, **417**, 925-929.
26. M. Chen, L. X. Zheng, B. Santra, H. Y. Ko, R. A. DiStasio, M. L. Klein, R. Car and X. F. Wu, *Nat. Chem.*, 2018, **10**, 413-419.
27. E. W. Hansen, R. Schmidt, M. Stocker and D. Akporiaye, *Microporous Mater.*, 1995, **5**, 143-150.
28. S. Takahara, M. Nakano, S. Kittaka, Y. Kuroda, T. Mori, H. Hamano and T. Yamaguchi, *J. Phys. Chem. B*, 1999, **103**, 5814-5819.
29. A. Faraone, L. Liu, C. Y. Mou, P. C. Shih, J. R. D. Copley and S. H. Chen, *J. Chem. Phys.*, 2003, **119**, 3963-3971.
30. T. Tsukahara, W. Mizutani, K. Mawatari and T. Kitamori, *J. Phys. Chem. B*, 2009, **113**, 10808-10816.
31. R. Sato, S. Ohkuma, Y. Shibuta, F. Shimojo and S. Yamaguchi, *J. Phys. Chem. C*, 2015, **119**, 28925-28933.
32. M.-H. Du, A. Kolchin and H.-P. Cheng, *J. Chem. Phys*, 2004, **120**, 1044-1054.
33. N. Kumar, P. R. C. Kent, A. V. Bandura, J. D. Kubicki, D. J. Wesolowski, D. R. Cole and J. O. Sofo, *J. Chem. Phys.*, 2011, **134**.
34. M.-P. Gaigeot, M. Sprik and M. Sulpizi, *J. Phys.: Condens. Matter*, 2012, **24**.
35. G. Tocci and A. Michaelides, *J. Phys. Chem. Lett.*, 2014, **5**, 474-480.
36. R. Osuga, T. Yokoi, K. Doitomi, H. Hirao and J. N. Kondo, *J. Phys. Chem. C*, 2017, **121**, 25411-25420.
37. L. R. Merte, G. Peng, R. Bechstein, F. Rieboldt, C. A. Farberow, L. C. Grabow, W. Kudernatsch, S. Wendt, E. Lægsgaard, M. Mavrikakis and F. Besenbacher, *Science*, 2012, **336**, 889-893.
38. M. Nogami, H. Matsushita, Y. Goto and T. Kasuga, *Adv. Mater.*, 2000, **12**, 1370-1372.
39. Y. Daiko, T. Kasuga and M. Nogami, *Chem. Mater.*, 2002, **14**, 4624-4627.
40. L. Malavasi, C. A. J. Fisher and M. S. Islam, *Chem. Soc. Rev.*, 2010, **39**, 4370-4387.

41. M. D. Fayer, D. E. Moilanen, D. Wong, D. E. Rosenfeld, E. E. Fenn and S. Park, *Acc. Chem. Res.*, 2009, **42**, 1210-1219.
42. C. Pantalei, R. Senesi, C. Andreani, P. Sozzani, A. Comotti, S. Bracco, M. Beretta, P. Sokol and G. Reiter, *Phys. Chem. Chem. Phys.*, 2011, **13**, 6022-6028.
43. S. Parashar, D. Lesnicki and M. Sulpizi, *J. Phys. Chem. Lett.*, 2018, **9**, 2186-2189.
44. M. Sulpizi, M.-P. Gaigeot and M. Sprik, *J. Chem. Theory Comput.*, 2012, **8**, 1037-1047.
45. Y. Kazoe, K. Mawatari, Y. Sugii and T. Kitamori, *Anal. Chem.*, 2011, **83**, 8152-8157.
46. C. C. Chang, Y. Kazoe, K. Morikawa, K. Mawatari, R. J. Yang and T. Kitamori, *Anal. Chem.*, 2013, **85**, 4468-4474.
47. S. Ong, X. Zhao and K. B. Eisenthal, *Chem. Phys. Lett.*, 1992, **191**, 327-335.
48. K. Leung, I. M. B. Nielsen and L. J. Criscenti, *J. Am. Chem. Soc.*, 2009, **131**, 18358-18365.
49. J. C. Fogarty, H. M. Aktulga, A. Y. Grama, A. C. T. van Duin and S. A. Pandit, *J. Chem. Phys.*, 2010, **132**, 174704.
50. A. A. Hassanali and S. J. Singer, *J. Phys. Chem. B*, 2007, **111**, 11181-11193.
51. P. Leroy, N. Devau, A. Revil and M. Bizi, *J. Coll. Inter. Sci.*, 2013, **410**, 81-93.
52. G. K. Lockwood and S. H. Garofalini, *J. Chem. Phys.*, 2009, **131**, 074703.
53. K. L. Geisinger, G. V. Gibbs and A. Navrotsky, *Phys. Chem. Minerals*, 1985, **11**, 266-283.
54. K. Vanheusden, P. P. Korambath, H. A. Kurtz, S. P. Karna, D. M. Fleetwood, W. M. Shedd and R. D. Pugh, *IEEE Trans. Nucl. Sci.*, 1999, **46**, 1562-1567.
55. J. Godet, F. Giustino and A. Pasquarello, *Phys. Rev. Lett.*, 2007, **99**.
56. T. S. Mahadevan and S. H. Garofalini, *J. Phys. Chem. B*, 2007, **111**, 8919-8927.
57. T. S. Mahadevan and S. H. Garofalini, *J. Phys. Chem. C*, 2008, **112**, 1507-1515.
58. G. K. Lockwood and S. H. Garofalini, *J. Phys. Chem. C*, 2014, **118**, 29750-29759.
59. S. Xu, G. W. Scherer, T. S. Mahadevan and S. H. Garofalini, *Langmuir*, 2009, **25**, 5076-5083.
60. M. Kagan, G. K. Lockwood and S. H. Garofalini, *Phys. Chem. Chem. Phys.*, 2014, **16**, 9294-9301.
61. J. Lentz and S. H. Garofalini, *Phys. Chem. Chem. Phys.*, 2018, **20**, 16414-16427.
62. A. Rimola, D. Costa, M. Sodupe, J.-F. Lambert and P. Ugliengo, *Chem. Rev.*, 2013, **113**, 4216-4313.
63. M. J. Wiedemair, M. Hitzenberger and T. S. Hofer, *Phys. Chem. Chem. Phys.*, 2015, **17**, 10934-10943.
64. M. J. Wiedemair and T. S. Hofer, *Phys. Chem. Chem. Phys.*, 2017, **19**, 31910-31920.
65. J. Yeon and A. C. T. van Duin, *J. Phys. Chem. C*, 2015, **120**, 305-317.
66. J. M. Rimza, J. Yeon, A. C. van Duin and J. Du, *J. Phys. Chem. C*, 2016, **120**, 24803-24816.
67. T. Hofer, M. Hitzenberger and B. Randolf, *J. Chem. Theory Comput.*, 2012, **8**, 3586-3595.
68. G. Bussi, D. Donadio and M. Parrinello, *J. Chem. Phys.*, 2007, **126**, 014107.
69. G. Cassone, F. Creazzo, P. V. Giaquinta, J. Sponer and F. Saija, *Phys. Chem. Chem. Phys.*, 2017, **19**, 20420-20429.
70. R. H. Henchman and S. J. Irudayam, *J. Phys. Chem. B*, 2010, **114**, 16792-16810.
71. S. H. Garofalini, T. S. Mahadevan, S. Xu and G. W. Scherer, *ChemPhysChem*, 2008, **9**, 1997-2001.
72. W. B. Holzapfel, *J. Chem. Phys.*, 1969, **50**, 4424-4428.
73. E. Schwegler, G. Galli, F. Gygi and R. Q. Hood, *Phys. Rev. Lett.*, 2001, **87**, 265501-265501-265504.
74. N. Uddin, J. Kim, B. J. Sung, T. H. Choi and C. H. Choi, *J. Phys. Chem. B*, 2014, **118**, 13671-13678.
75. J. Godet and A. Pasquarello, *Phys. Rev. Lett.*, 2006, **97**.
76. A. Pasquarello and R. Car, *Phys. Rev. Lett.*, 1998, **80**, 5145-5147.

77. R. Vacha, R. Zangi, J. B. F. N. Engberts and P. Jungwirth, *J. Phys. Chem. C*, 2008, **112**, 7689-7692.
78. M. A. Wilson, A. Pohorille and L. R. Pratt, *J. Phys. Chem.*, 1987, **91**, 4873-4878.

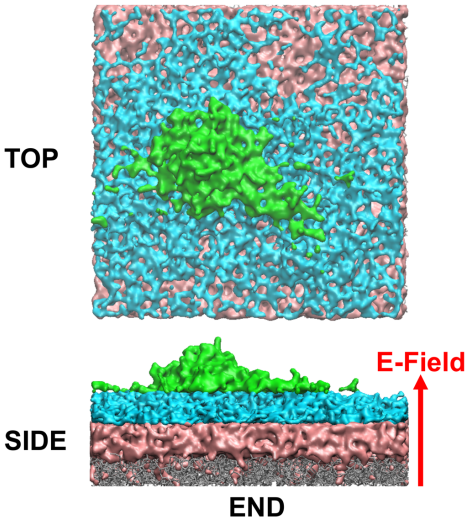

Table of Content Image:
Water 'layers' 1 and 2 in pink; 'layer' 3 in blue and green over portion of glass surface (grey). +90° field causes water migration and clustering.